Optimal borehole placement for the design of rectangular shallow foundation systems under undrained soil conditions: A stochastic framework

Danko J. Jerez[a], M. Chwała[b,*], Hector A. Jensen[a], Michael Beer[c,d,e]

[a]*Departamento de Obras Civiles, Universidad Técnica Federico Santa María, Avda. España 1680, Valparaíso 2390123, Chile*
[b]*Faculty of Civil Engineering, Wrocław University of Science and Technology, Wybrzeże Wyspiańskiego 27, 50-377 Wrocław, Poland*
[c]*Institute for Risk and Reliability, Leibniz Universität Hannover, Callinstr. 34, 30167 Hannover, Germany*
[d]*International Joint Research Center for Resilient Infrastructure & International Joint Research Center for Engineering Reliability and Stochastic Mechanics, Tongji University, 1239 Siping Road, Shanghai 200092, China*
[e]*Institute for Risk and Uncertainty and School of Engineering, University of Liverpool, Peach Street, Liverpool L69 7ZF, UK*

Abstract

This contribution proposes a framework to identify optimal borehole configurations for the design of shallow foundation systems under undrained soil conditions. To this end, the minimization of a performance measure defined in terms of the bearing capacity standard deviations is considered. The random failure mechanism method is adopted for random bearing capacity evaluation, thereby enabling explicit treatment of soil spatial variability with tractable numerical efforts. A sampling-based optimization scheme is implemented to account for the non-smooth nature of the resulting objective function. The proposed framework provides non-trivial sensitivity information of the chosen performance measure as a byproduct of the solution process. Further, the method allows assessing the effect of increasing the number of soil soundings into the standard deviations of bearing capacity estimates. Three cases involving different foundation layouts are studied to illustrate the capabilities of the approach. Numerical results suggest that the herein proposed framework can be potentially adopted as a supportive tool to determine optimal soil sounding strategies for the design of a practical class of civil engineering systems.

Keywords: Random failure mechanism method, Optimal borehole placement, Soil spatial variability, Spatial averaging, Transitional Markov chain Monte Carlo

1. Introduction

Site investigation programs play an instrumental role in the design of geotechnical engineering systems [1–4]. In this regard, soil sounding techniques such as cone penetration tests (CPTs) [5]

E-mail: marcin.chwala@pwr.edu.pl (M. Chwała)

represent the prevalent approach to determine relevant geotechnical properties in a plethora of applications [6–11]. Despite the high-quality information that soil soundings can usually provide, soils undergo considerable changes over time and space due to the complex geological processes involved in their natural formation (see, e.g., [12–16]). Therefore, the consideration of the spatial variability of soil properties is of the utmost importance to obtain meaningful results when devising borehole placement strategies for site investigation.

Some of the available methodologies to determine optimal soil sampling schemes aim to maximize their robustness in terms of soil strength parameter identification [17–20]. While these approaches have proved effective in characterizing soil properties from a general perspective, an alternative class of methods focus on specialized soil sampling strategies tailored to specific geotechnical applications. In this regard, the consideration of the target system behavior constitutes an essential component in the formulation of such methods. Specifically, ad hoc approaches have been proposed for, e.g., slope stability assessment [21–26], foundation settlement prediction [27], and foundation bearing capacity analysis under plane-strain conditions [28]. Nonetheless, optimal borehole placement for the design of multiple shallow foundations considering the three-dimensional variability of soil properties has received relatively little attention.

Boreholes must be allocated within a given site to reduce the variability of bearing capacity estimates for the design of shallow foundation systems supported by spatially variable soil. In general, random bearing capacity evaluation has relied on coupling well-established methodologies for the analysis of foundation systems, such as the finite element method, with the use of random fields for characterizing the relevant properties of the supporting soil; see, indicatively, [13, 29–34]. Within this context, the information provided by CPTs can be explicitly incorporated by using, for instance, conditional random fields [35–37]. Despite the flexibility and generality of such strategies, one of their main drawbacks relates to the considerable computational overhead arising in their application, especially in three-dimensional cases [38]. To address this issue, the random failure mechanism method (RFMM) [39, 40] encompasses several attractive features pertaining to its practical implementation. By resorting to the kinematic method of limit analysis [41, 42] and the spatial averaging technique [43], random bearing capacities can be evaluated in a numerically tractable fashion while explicitly and rigorously accounting for the three-dimensional variability of soil properties. Even though the RFMM allows considering the effect of soil soundings on random bearing capacities [44–46], the practical implementation of the method has been mostly limited

to cases involving a single borehole. Thus, it is believed that there is still room for further developments in this area, particularly in the development of effective methods for identifying optimal borehole configurations in cases involving multiple foundations and multiple soil soundings.

This contribution presents an approach for optimal borehole placement in the context of rectangular shallow foundation design considering spatially variable and undrained soil conditions. In this regard, the optimal borehole placement problem is stated as the minimization of a performance measure defined in terms of the second-order statistics of the bearing capacities [46]. To evaluate the performance of different soil sounding configurations, the RFMM is adopted. A stochastic search technique based on an equivalent sampling problem [47, 48] is implemented to account for the non-smooth nature of the corresponding optimization problem. The proposed framework can be construed as an extension of the developments presented in [45, 46] and, moreover, as an alternative area of application of advanced simulation techniques [47]. Furthermore, the resulting approach entails the following features. First, it allows considering multiple foundations, multiple soil soundings, and the three-dimensional variability of soil properties. Second, instead of a single final solution, a set of nearly-optimal borehole configurations are generated. This, in turn, provides valuable insight about the problem at hand and improved flexibility for decision-making processes. Third, the method can be implemented to assess the tradeoff between the number of soil soundings and the reduction of the variability of foundation bearing capacities. Finally, the sensitivity of final configurations with respect to, e.g., the spatial correlation of undrained shear strength can be evaluated by virtue of the proposed approach. These types of analysis can be particularly valuable in the rather common cases where limited prior knowledge about the spatial correlation of soil properties is available. Numerical results suggest that the method presented in this contribution can identify borehole configurations that effectively reduce the variability of bearing capacity estimates. Overall, the herein proposed framework can be potentially adopted as a supportive tool to design site investigation programs and, in this manner, aid decision makers to enhance the safety and reliability of shallow foundation systems.

The organization of the paper is as follows. Section 2 states the optimal borehole placement problem and the performance measures under consideration. A brief description of the RFMM is provided in Section 3, while Section 4 summarizes the main characteristics of the adopted stochastic optimization scheme. Some practical implementation aspects are discussed in Section 5. Three cases involving different foundation systems are studied in Section 6 to illustrate the applicabil-

ity of the proposed approach. The paper closes with some final remarks and potential research directions.

2. Problem description

2.1. Probabilistic site characterization

Consider a soil under undrained conditions. In this case, the soil resistance is characterized in terms of the undrained shear strength, c_u, which can be represented in terms of a three-dimensional random field to account for its spatial variability [13]. In particular, a stationary log-normal random field with mean value μ_{c_u}, standard deviation σ_{c_u}, and Gaussian correlation structure is assumed in this contribution. Then, the covariance between two arbitrary points $\mathbf{p}_i = [x_i, y_i, z_i]$ and $\mathbf{p}_j = [x_j, y_j, z_j]$ is given by

$$C(\mathbf{p}_i, \mathbf{p}_j) = \sigma_{c_u}^2 \exp\left\{ - \left[\left(\frac{x_i - x_j}{\theta_x/\sqrt{\pi}} \right)^2 + \left(\frac{y_i - y_j}{\theta_y/\sqrt{\pi}} \right)^2 + \left(\frac{z_i - z_j}{\theta_z/\sqrt{\pi}} \right)^2 \right] \right\} \tag{1}$$

where θ_x, θ_y and θ_z are the scales of fluctuation (SOF) along the x, y and z axes, respectively, where the z axis points in the direction of gravity. In passing, it is noted that some authors have encouraged the use of alternative covariance functions, such as the Whittle-Mattérn model (see, e.g., [49]). Nevertheless, previously reported results [46] suggest that optimal borehole configurations may not be strongly sensitive to the adopted covariance structure.

Assume that n_F rectangular footings with known location and geometry are to be supported by the soil under consideration. Then, the bearing capacity of the kth foundation, denoted by ζ_k, $k = 1, \ldots, n_F$, depends on the undrained shear strength of the soil and, therefore, is a random variable with mean value μ_{ζ_k} and standard deviation σ_{ζ_k}. It is noted that the joint distribution of ζ_k, $k = 1, \ldots, n_F$, is generally unknown and it depends on the random field characteristics and the usually involved relationship between bearing capacities and undrained shear strength.

2.2. Optimal borehole placement for foundation design

To provide information for the design of the system of n_F foundations, consider that a total of n_B soil soundings must be placed at the corresponding site. It is assumed that no soil soundings have been previously allocated at the site of interest, i.e., the locations of the n_B boreholes must be determined simultaneously. In this setting, the position of the mth borehole in the $x - y$ plane is denoted by $\mathbf{b}_m = [x_m^B, y_m^B]$, $m = 1, \ldots, n_B$, and the entire array is fully determined by

$\mathbf{b} = [\mathbf{b}_1, \ldots, \mathbf{b}_{n_B}]^{\mathrm{T}} \in \mathbb{R}^{n_b}$ with $n_b = 2n_B$. Then, the optimal borehole placement problem relates to identifying the positions of the n_B boreholes such that they yield the best possible information for the evaluation of the foundation bearing capacities. This task can be stated in a mathematical programming framework as

$$\begin{aligned} \min_{\mathbf{b}} \quad & f(\mathbf{b}) \\ \text{s.t.} \quad & b_i^L \leqslant b_i \leqslant b_i^U, \ i = 1, \ldots, n_b \end{aligned} \tag{2}$$

where $\mathbf{b} \in \mathbb{R}^{n_b}$ is the vector of decision (design) variables, $f(\mathbf{b})$ is a suitable objective function, and b_i^L and b_i^U are the lower and upper limits for the ith decision variable. The side constraints characterize the available region to place the boreholes. In addition, the objective function measures the performance of a given soil sounding arrangement in terms of the variability of bearing capacity estimates [46].

2.3. Performance measures

Since the variability levels of different bearing capacities are affected to different extents by any given soil sounding array, the choice of the objective function $f(\mathbf{b})$ is not straightforward for systems of multiple foundations. In this regard, and following some of the ideas discussed in [46], two different performance measures defined in terms of the standard deviations of the different bearing capacities are adopted in this contribution.

2.3.1. Average normalized standard deviation

The first performance measure is referred to as *average normalized standard deviation*, and it is defined as [46]

$$\bar{\sigma}^{\mathrm{avg}}(\mathbf{b}) = \frac{1}{n_F} \sum_{k=1}^{n_F} \frac{\sigma_{\zeta_k}(\mathbf{b})}{\sigma_{\zeta_k}^0} \tag{3}$$

where $\sigma_{\zeta_k}^0$ and $\sigma_{\zeta_k}(\mathbf{b})$ denote the standard deviation of the kth bearing capacity when no boreholes are included into the analysis (base scenario) and when the borehole configuration $\mathbf{b}$ is considered, respectively. The ratio $\sigma_{\zeta_k}(\mathbf{b})/\sigma_{\zeta_k}^0$, $k = 1, \ldots, n_F$, quantifies the variability level of the kth bearing capacity as a fraction of the unconditioned standard deviation. Thus, $\bar{\sigma}^{\mathrm{avg}}(\mathbf{b})$ can be related to the expected level of information gain. In general, $\bar{\sigma}^{\mathrm{avg}} \approx 1$ indicates negligible improvement, while $\bar{\sigma}^{\mathrm{avg}} < 1$ indicates an average reduction in the variability of the bearing capacities. By adopting this performance measure, the optimal borehole configuration yields the best average

improvement for all foundations, although it may privilege local information gain. That is, some bearing capacities may significantly reduce their variability while others may remain unaffected.

2.3.2. Maximum normalized standard deviation

The second performance measure is called *maximum normalized standard deviation*, and it is given by [46]

$$\bar{\sigma}^{\max}(\mathbf{b}) = \max_{k=1,\ldots,n_F} \left(\frac{\sigma_{\zeta_k}(\mathbf{b})}{\sigma^0_{\zeta_k}} \right) \tag{4}$$

where all terms have been previously defined. In this case, performance is quantified in terms of the maximum normalized variability level across all bearing capacities. Hence, this measure can be associated with the minimum level of information gain achieved by the soil sounding array. The corresponding optimal configurations usually tend to reduce all bearing capacity standard deviations to a similar extent, although significant local improvements can be disregarded by choosing this objective function. Furthermore, if the optimal configuration verifies $\bar{\sigma}^{\max} \approx 1$, then it can be argued that the current number of available soil soundings is unable to reduce the variability level of all bearing capacities in a simultaneous manner.

3. Random bearing capacity assessment

Following the previous presentation, it is noted that the performance of a given soil sounding configuration is measured in terms of the standard deviations of the foundation bearing capacities. As already pointed out, the evaluation of such standard deviations is not straightforward when three-dimensional random fields are adopted to characterize geotechnical properties [50]. To address this task, an efficient approach called random failure mechanism method (RFMM) is adopted [39]. The distinctive feature of the RFMM is that it enables random bearing capacity evaluation considering the three-dimensional variability of soil properties in a numerically tractable fashion. A brief description of the approach is presented in this section.

3.1. Failure mechanisms and spatial averaging

The kinematic method of limit analysis plays an instrumental role in the formulation of the RFMM [39], where suitable failure mechanisms are employed to evaluate the capacity of the system of interest (see, e.g., [40, 51]). For simplicity, only rough-based foundations are considered in this contribution, and the Prandtl-type mechanism introduced in [52] is adopted for bearing capacity assessment. Figure 1 shows this failure mechanism type, which involves $n_R = 30$ dissipation

regions (surfaces and volumes). The ith dissipation region of the kth foundation, denoted by $R_{k,i}$, is associated with a constant (averaged) undrained soil strength $\bar{c}_{u,R_{k,i}}$, $i = 1, \ldots, n_R$, $k = 1, \ldots, n_F$. For a given value of $\bar{\mathbf{c}}_{u,\mathbf{R}_k} = [\bar{c}_{u,R_{k,1}}, \ldots, \bar{c}_{u,R_{k,n_R}}]$, the failure mechanism geometry that minimizes the corresponding ultimate load yields the actual bearing capacity of the foundation (see Appendix A). In this manner, the bearing capacities ζ_k, $k = 1, \ldots, n_F$, can be computed in terms of the averaged undrained shear strengths, i.e., $\bar{\mathbf{c}}_{u,\mathbf{R}} = [\bar{\mathbf{c}}_{u,\mathbf{R}_1}, \ldots, \bar{\mathbf{c}}_{u,\mathbf{R}_{n_F}}]^{\mathrm{T}} \in \mathbb{R}^{n_T}$ with $n_T = n_F n_R$.

To account for the spatial variability of c_u, which is represented as a stationary lognormal random field (see Section 2.1), the vector $\bar{\mathbf{c}}_{u,\mathbf{R}}$ is assumed to follow a lognormal distribution with a certain correlation structure [39, 40, 43, 51]. Specifically, and employing concepts from Vanmarcke's spatial averaging [43], the vector $\bar{\mathbf{c}}_{u,\mathbf{R}}$ has mean value μ_{c_u} and covariance matrix $\mathbf{\Sigma_{RR}} \in \mathbb{R}^{n_T \times n_T}$. The latter is determined in terms of the chosen covariance function and the geometry of the failure mechanisms associated with $c_u = \mu_{c_u}$ [53]. Then, Monte Carlo simulation can be employed to estimate the unconditioned standard deviations of the bearing capacities, i.e., $\sigma^0_{\zeta_k}$, $k = 1, \ldots, n_F$. The only restriction of the approach is that the distance between the different foundations must be sufficiently large to ensure that the failure mechanisms are not interfering with each other [46]. This implies that, in practice, mechanical interaction between foundations cannot be fully considered within this formulation.

3.2. Consideration of boreholes

In the RFMM, the information provided by soil soundings can be incorporated as probabilistic conditions on the random field [44]. Each borehole is represented as a straight vertical line, while the undrained shear strengths at the boreholes are taken as n_B correlated lognormal random variables contained in $\bar{\mathbf{c}}_{u,\mathbf{B}} = [\bar{c}_{u,B_1}, \ldots, \bar{c}_{u,B_{n_B}}]$ with mean value μ_{c_u}, standard deviation $\gamma\sigma_{c_u}$, and covariance matrix $\mathbf{\Sigma_{BB}}(\mathbf{b}) \in \mathbb{R}^{n_B \times n_B}$. In this formulation, γ is a small positive constant introduced to reflect measurement accuracy. Specifically, the value $\gamma = 0.01$ is adopted [44–46]. Hence, the vector $\bar{\mathbf{c}}_u = [\bar{\mathbf{c}}_{u,\mathbf{R}}, \bar{\mathbf{c}}_{u,\mathbf{B}}]^{\mathrm{T}} \in \mathbb{R}^{n_c}$ comprises $n_c = n_T + n_B$ correlated lognormal random variables with mean value μ_{c_u} and covariance matrix given by

$$\mathbf{\Sigma}(\mathbf{b}) = \begin{bmatrix} \mathbf{\Sigma_{RR}} & \mathbf{\Sigma_{BR}}(\mathbf{b})^{\mathrm{T}} \\ \mathbf{\Sigma_{BR}}(\mathbf{b}) & \mathbf{\Sigma_{BB}}(\mathbf{b}) \end{bmatrix} \tag{5}$$

where $\boldsymbol{\Sigma}_{\mathbf{BR}}(\mathbf{b}) \in \mathbb{R}^{n_B \times n_T}$ is the cross-covariance matrix between $\bar{\mathbf{c}}_{u,\mathbf{B}}$ and $\bar{\mathbf{c}}_{u,\mathbf{R}}$. The matrices $\boldsymbol{\Sigma}_{\mathbf{BR}}(\mathbf{b})$ and $\boldsymbol{\Sigma}_{\mathbf{BB}}(\mathbf{b})$ are also computed using spatial averaging [43, 46]. Once $\boldsymbol{\Sigma}(\mathbf{b})$ is obtained, Monte Carlo simulation is carried out to estimate the standard deviations $\sigma_{\zeta_k}(\mathbf{b})$, $k = 1, \ldots, n_F$.

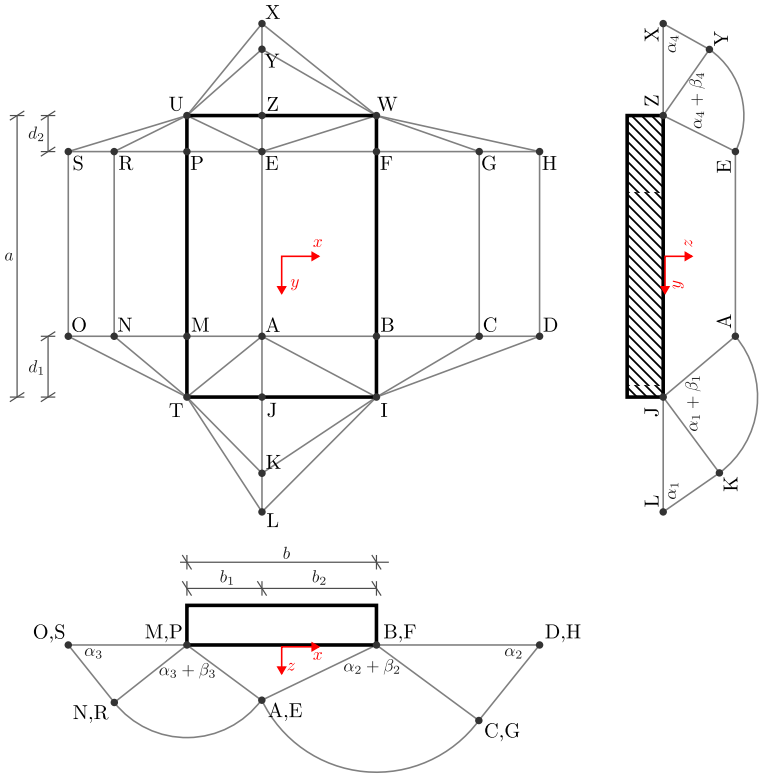

Figure 1: Sketch of the failure mechanism type under consideration (rough-based foundation).

3.3. Basic procedure

For clarity and completeness, the basic steps of the sampling procedure to estimate the standard deviations of the n_F bearing capacities, conditioned on a given array of boreholes $\mathbf{b}$, are provided in the following. A thorough description of this method, including a detailed algorithm to obtain realizations of $\bar{\mathbf{c}}_u$, can be found in [46].

1. Compute the covariance matrix $\boldsymbol{\Sigma}(\mathbf{b})$ in Eq. (5) using spatial averaging [43].
2. Perform direct Monte Carlo simulation. For $\ell = 1, \ldots, N_S$:
   (a) Generate a realization $\bar{\mathbf{c}}_u^{(\ell)}$ of $\bar{\mathbf{c}}_u$. This is carried out using, e.g., the Cholesky decomposition method [13] in a suitable underlying Gaussian space [46].
   (b) Evaluate the corresponding realizations of the bearing capacities, $\zeta_k^{(\ell)} = \zeta_k(\bar{\mathbf{c}}_u^{(\ell)})$, $k = 1, \ldots, n_F$, according to Appendix A.

3. Estimate the standard deviations of the foundation bearing capacities as

$$\sigma_{\zeta_k}(\mathbf{b}) \approx \hat{\sigma}_{\zeta_k}(\mathbf{b}) = \left[\frac{1}{N_S - 1} \sum_{\ell=1}^{N_S} \left(\zeta_k^{(\ell)} - \frac{1}{N_S} \sum_{\kappa=1}^{N_S} \zeta_k^{(\kappa)} \right)^2 \right]^{1/2}, \quad k = 1, \ldots, N_F \tag{6}$$

Then, the standard deviation estimates can be used to obtain an estimate of the objective function $f(\mathbf{b})$. In this manner, computationally intensive procedures for bearing capacity assessment are circumvented while fully accounting for the three-dimensional variability of the undrained shear strength.

4. Stochastic optimization approach

The objective function $f(\mathbf{b})$ in Eq. (2) is evaluated in terms of Monte Carlo estimates and, therefore, it presents an inherent variability that must be properly considered during the solution process [54]. Moreover, the performance measures defined in Section 2.3 may lead to multiple local optima or multiple discontinuous, nearly-optimal regions [46]. To account for these issues, the use of stochastic search techniques proves a particularly useful and robust solution approach [55]. In particular, a stochastic optimization strategy based on an equivalent sampling problem [47, 48, 56] is implemented in this contribution.

4.1. Equivalent sampling problem

According to the simulated annealing concept [57], minimizing $f(\mathbf{b})$ is equivalent to finding the maximum of $\exp(-f(\mathbf{b})/T)$, $T > 0$. Then, consider the auxiliary non-normalized distribution [47, 58, 59]

$$p(\mathbf{b}; T) \propto U_{\boldsymbol{\mathcal{B}}}(\mathbf{b}) \exp\left(-\frac{f(\mathbf{b})}{T} \right) \tag{7}$$

where $T > 0$ is the so-called temperature parameter and $U_{\boldsymbol{\mathcal{B}}}(\mathbf{b})$ is a uniform distribution over the set $\boldsymbol{\mathcal{B}} = \{\mathbf{b} \in \mathbb{R}^{n_b} : b_i^L \leqslant b_i \leqslant b_i^U, i = 1, \ldots, n_b\}$. The artificial treatment of $\mathbf{b}$ as random variables is merely a tool for the formulation of the method. In this setting, the parameter T plays a key role in determining the shape of the auxiliary distribution. Higher values of T lead to flatter distributions and, when $T \to \infty$, the auxiliary distribution becomes uniform over the search space, i.e., $\lim_{T\to\infty} p(\mathbf{b}; T) = U_{\boldsymbol{\mathcal{B}}}(\mathbf{b})$. Conversely, reducing the value of T renders distributions that are more concentrated around designs that yield lower values of $f(\mathbf{b})$. In the limit case, the probability mass is densely concentrated in a vicinity of the optimal solution set $\boldsymbol{\mathcal{B}}_f^*$, i.e.,

the set of designs that minimize the objective function. That is, $\lim_{T\to 0} p(\mathbf{b};T) = U_{\boldsymbol{\mathcal{B}}_f^*}(\mathbf{b})$. Thus, the solution of the Eq. (2) can be stated as the equivalent problem of sampling from the target distribution $p^*(\mathbf{b}) = \lim_{T\to 0} p(\mathbf{b};T)$. Furthermore, this formulation can be also interpreted as a Bayesian model updating problem in which $U_{\boldsymbol{\mathcal{B}}}(\mathbf{b})$ plays the role of the prior distribution and $\exp\left(-f(\mathbf{b})/T\right)$, $T \to 0$, of the (non-normalized) likelihood function [47].

4.2. Stochastic simulation method

To obtain samples (designs) distributed according to $p^*(\mathbf{b})$, a sequential sampling strategy is adopted [58–60]. Consider the sequence of non-normalized intermediate distributions

$$\begin{aligned} &p_0(\mathbf{b}) = U_{\boldsymbol{\mathcal{B}}}(\mathbf{b}) && (T_0 \to \infty) \\ &p_j(\mathbf{b}) \propto U_{\boldsymbol{\mathcal{B}}}(\mathbf{b}) \exp\left(-\frac{f(\mathbf{b})}{T_j}\right), && j = 1,\ldots,J \end{aligned} \tag{8}$$

where $\infty = T_0 > T_1 > \cdots > T_J \to 0$ is a sequence of monotonically decreasing temperatures. These distributions are increasingly concentrated near the optimal solution set $\boldsymbol{\mathcal{B}}_f^*$. In this regard, the idea is to achieve a gradual transition from a uniform distribution over the search space ($j = 0$) to a distribution with a sufficiently low temperature ($T_J \to 0$). A sequential generation of samples is performed to this end, whereby the initial samples are uniformly distributed over $\boldsymbol{\mathcal{B}}$ and the final designs densely populate a vicinity of $\boldsymbol{\mathcal{B}}_f^*$ [47].

To carry out the sampling process, the transitional Markov chain Monte Carlo (TMCMC) method [60] is adopted. In the initial stage ($j = 0$), a set of designs $\{\mathbf{b}_0^{(n)}, n = 1,\ldots,N\}$ uniformly distributed over $\boldsymbol{\mathcal{B}}$ are generated using direct Monte Carlo simulation. Thereafter, the samples $\{\mathbf{b}_j^{(n)}, n = 1,\ldots,N\}$ at stage $j = 1,2,\ldots,J$ are obtained using the Metropolis-Hastings (M-H) algorithm [61, 62]. Several independent chains with stationary distribution $p_j(\mathbf{b})$ are generated at stage j, whose initial states are drawn from the samples at stage $j-1$ using importance sampling and resampling concepts. With the aim to achieve a smooth transition between consecutive distributions, the temperature parameter T_j is adaptively defined to satisfy the condition [47, 58]

$$\sum_{n=1}^{N} \exp\left[-2(T_j^{-1} - T_{j-1}^{-1}) f(\mathbf{b}_{j-1}^{(n)})\right] = \frac{1}{\nu N}\left(\sum_{n=1}^{N} \exp\left[-(T_j^{-1} - T_{j-1}^{-1}) f(\mathbf{b}_{j-1}^{(n)})\right]\right)^2 \tag{9}$$

where $\nu \in (0,1)$ is the so-called effective sample size parameter [58]. If the current c.o.v. estimate of the objective function is sufficiently small or a maximum number of stages is completed, the

sampling process is stopped [47]. Then, the final designs can be regarded as nearly optimal solutions. That is, a number of nearly equivalent borehole arrays are obtained rather than a unique final configuration of soil soundings, which can provide improved flexibility for decision-making purposes. Nevertheless, if a single solution is required, the design with the smallest objective function value can be chosen. In addition, the sets of samples generated during the different stages provide valuable insight about the sensitivity of the objective function with respect to the decision variables [47, 56].

5. Implementation aspects

5.1. Evaluation of the objective function

The proposed framework relies on the sequential generation of designs to populate a vicinity of the optimal solution set. In this regard, three relevant aspects in the estimation of the objective function $f(\mathbf{b})$ are considered. The first pertains to the computation of the covariance matrix $\boldsymbol{\Sigma}(\mathbf{b})$ in Eq. (5), which is one of the most numerically demanding tasks of the RFMM [39]. Since the submatrix $\boldsymbol{\Sigma}_{\mathbf{RR}}$ does not depend on the borehole positions, it can be computed offline, i.e., before the optimization process is carried out. Hence, only the submatrices $\boldsymbol{\Sigma}_{\mathbf{BR}}(\mathbf{b})$ and $\boldsymbol{\Sigma}_{\mathbf{BB}}(\mathbf{b})$ are updated for each soil sounding configuration, which allows significant computational savings. The second aspect corresponds to select an appropriate value of N_S (see Section 3.3) to achieve a suitable tradeoff between computational cost and quality of the objective function estimates. Even though the optimal value of N_S is problem-dependent, the choice $N_S > 200$ has yielded satisfactory results for the examples addressed in this contribution. In passing, it is noted that bearing capacity evaluation is significantly less demanding than computing $\boldsymbol{\Sigma}(\mathbf{b})$. Finally, the customary technique of using common random numbers [55] is implemented. That is, the same stream of pseudorandom numbers is used to estimate $f(\mathbf{b})$ at different values of $\mathbf{b}$. In this manner, the negative impact of the variability of the objective function estimates on the optimization process can be effectively reduced.

5.2. Adaptive surrogate model

Following some of the ideas discussed in [48, 63], an adaptive surrogate model for the objective function is implemented. The standard deviations are approximated using kriging interpolants [64, 65] as $\sigma_{\zeta_k}(\mathbf{b}) \approx \sigma^{\mathrm{kr}}_{\zeta_k}(\mathbf{b})$, $k = 1, \ldots, n_F$. In this framework, underlying Gaussian processes defined in terms of available data points are employed to approximate the target functions [64].

Some of the advantages of kriging are that (i) a regular grid of support points is not needed, (ii) the prediction at the support points are exact, and (iii) an estimate of the prediction c.o.v. is available. Furthermore, due to the annealing properties of the optimization technique, the effective support of the current distribution is usually contained in those of preceding distributions [56]. Hence, support points retrieved throughout the different stages of the method can be employed to approximate the objective function by means of kriging surrogates.

Based of the previous features, a local and adaptive surrogate model strategy is formulated as follows. First, a database of support points is initialized using, e.g., Latin Hypercube sampling over the initial search space $\boldsymbol{\mathcal{B}}$. Then, kriging metamodels based on N_{sp} support points are employed to approximate the standard deviations. In the initial stage, which corresponds to direct Monte Carlo simulation, the N_{sp} database points that are closer to the evaluated design $\mathbf{b}$ are considered as support points. For the next stages, which involve the M-H algorithm, the support points are kept constant for each chain and they correspond to the N_{sp} points closer to the starting (seed) sample. This is done to circumvent potential discontinuities of the objective function surrogate associated with slightly different sets of support points for consecutive chain states [63]. The predictions for a given borehole configuration $\mathbf{b}$ are only accepted if:

1. The design $\mathbf{b}$ lies within the n_b-dimensional convex hull of the N_{sp} support points.
2. The kriging predictions have a corresponding c.o.v. below a user-defined threshold ϵ.
3. Every kriging prediction is larger than its corresponding Q-quantile in the database.

The three previous criteria aim to control the quality of the surrogate model [56, 63]. If any of these conditions is not met, the kriging prediction is rejected. Then, the standard deviations are directly evaluated using the RFMM, and the point $\mathbf{b}$ is added to the database. Hence, additional support points that lie closer to the optimal solution set are incorporated as new designs near such set are generated. In general, this strategy can significantly improve the numerical efficiency of the approach without compromising the quality of the optimization results [48]. However, alternative surrogate strategies can also be considered within the proposed framework.

5.3. Parallelization strategies

The TMCMC method presents advantageous features for practical implementation in high-performance computing environments [63]. In this regard, the initial stage corresponds to direct Monte Carlo simulation and, therefore, it can be fully scheduled in parallel. Thereafter, each stage

produces a set of Markov chains that are independent between each other. Hence, the simulation of each chain can be carried out independently by a single computer worker and, in this manner, it becomes possible to generate the entire set of Markov chains in parallel using a pool of computer workers. Based on the preceding discussion, it is seen that the entire optimization process can be performed using parallelization techniques, which may help to improve the overall computational efficiency of the proposed framework [56].

Surrogate model techniques and parallelization strategies can be jointly implemented, for which a balance must be achieved between the adaptability of the database of support points and the effectiveness of the parallelization process. To this end, the samples at each stage can be generated in batches [48]. That is, a total of N_{par} samples are simultaneously generated, and then the database of support points is updated with the corresponding designs that were evaluated using the RFMM. The value of N_{par} should be relatively small to update the database on a regular basis, but large enough to ensure the effectiveness of the parallelization process. This procedure is repeated until the required sample size N is reached. In addition, since the computational cost of estimating $f(\mathbf{b})$ depends on whether the corresponding kriging prediction is accepted or rejected, dynamic scheduling schemes can be beneficial to distribute the function evaluations on a first-come-first-serve basis [63]. Overall, the previously described implementation allows exploiting the parallelization properties of the TMCMC method while retaining the adaptability of the surrogate model strategy.

6. Application examples

Three different examples are studied in this section. Specifically, the identification of optimal soil sounding locations for the three foundation arrays shown in Fig. 2 is considered to evaluate the capabilities of the proposed framework. These include a single rectangular foundation (see Fig. 2-a), a symmetrical system of four identical squared footings (see Fig. 2-b), and a non-symmetrical array of four foundations with different sizes (see Fig. 2-c). The figure also indicates the feasible region to allocate the available boreholes for each foundation system.

In all examples, the number of available soil soundings, n_B, ranges from one to five. The undrained shear strength of the soil is characterized by means of a lognormal random field with mean value $\mu_{c_u} = 100$ kPa and standard deviation $\sigma_{c_u} = 0.5\mu_{c_u}$. In all cases under consideration, different values for the horizontal fluctuation scale are considered such that $\theta_h \in [1, 20]$ m, whereas

the vertical fluctuation scale is taken as $\theta_v = 1$ m unless otherwise stated. Regarding the numerical implementation of the RFMM (see Section 3), a total of $N_S = 500$ realizations are considered for the evaluation of the objective function. In the context of the adopted search technique (see Sections 4 and 5), and based on some of the ideas discussed in [47, 48], the number of designs per stage is defined as $N = 300n_B$, the parameter value $\nu = 0.5$ is adopted, the initial kriging database comprises the initial set of designs, a total of $N_{\text{sp}} = 10n_B$ support points are considered for the implementation of the metamodel, the surrogate acceptance criteria consider $Q = 0.05$ and $\epsilon = 0.10$, and batches of $N_{\text{par}} = 100$ designs are evaluated in parallel during each stage. It is noted that validation calculations have indicated that this selection of parameter values is adequate for the examples studied in this contribution.

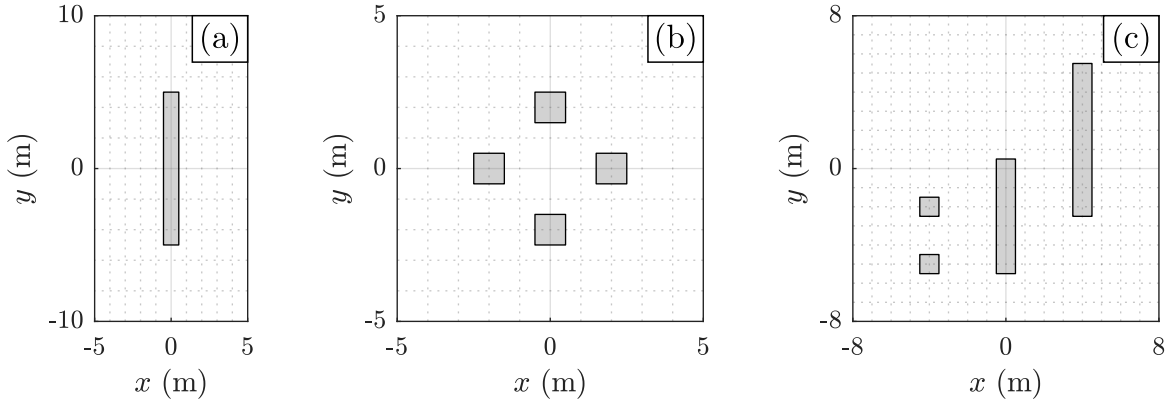

Figure 2: Foundation layouts and feasible regions considered in the different examples. (a) Example 1. (b) Example 2. (c) Example 3.

6.1. Example 1

This example aims to demonstrate the main features of the proposed approach in a relatively simple foundation system, namely, a single rectangular footing of width equal to 1 m and length equal to 10 m. In this case, the two performance measures defined in Section 2.3 are equivalent. Hence, the objective function in Eq. (2) becomes $f(\mathbf{b}) = \bar{\sigma}_\zeta(\mathbf{b}) = \sigma_\zeta(\mathbf{b})/\sigma_\zeta^0$, where $\sigma_\zeta(\mathbf{b})$ is the bearing capacity standard deviation corresponding to the borehole configuration $\mathbf{b}$, σ_ζ^0 is the base or unconditioned standard deviation of the bearing capacity, and $\bar{\sigma}_\zeta(\mathbf{b})$ is the normalized standard deviation of the bearing capacity.

First, a single available soil sounding is considered with horizontal fluctuation scale $\theta_h = 5$ m, which leads to a ratio between horizontal fluctuation scale and foundation length equal to 0.5. The set of decision (design) variables is then expressed as $\mathbf{b} = [x_b, y_b]^{\text{T}}$, where x_b and y_b are, respectively,

the x and y coordinates of the borehole. For reference purposes, Fig. 3 presents the contours of the normalized standard deviation of the bearing capacity in terms of the borehole coordinates. These contours have been obtained by generating a set of estimates of $f(\mathbf{b})$ corresponding to alternative soil sounding locations distributed over the entire search space. The resulting curves, which are fairly rugged due to the inherent variability of Monte Carlo estimates, have been smoothed to enhance the representation of the objective function behavior. From the figure, it seems that $f(\mathbf{b})$ is minimized for boreholes located near the foundation center, i.e., $\mathbf{b} = [0, 0]$. This outcome, which can be regarded as rather intuitive, agrees quite well with previously reported findings (see, indicatively, [44, 46]). In addition, the contours around this region are mainly aligned with the y axis, that is, the function $f(\mathbf{b})$ seems to be more sensitive to the x coordinate of the borehole than to its y coordinate near the foundation center.

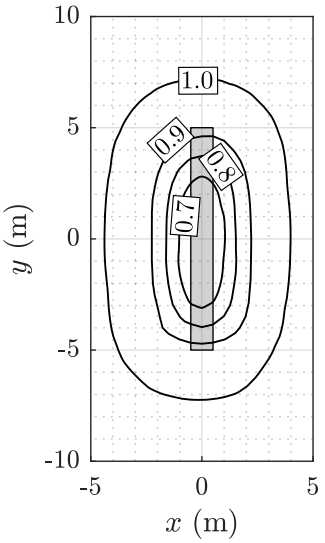

Figure 3: Contours of the normalized standard deviation, $\bar{\sigma}_\zeta(\mathbf{b})$, in terms of the borehole coordinates. Example 1.

Following the presentation in Section 4, a stochastic search strategy is implemented to determine a set of nearly-optimal locations for the available soil sounding. For illustration purposes, a total of nine sampling stages ($J = 8$) are considered. As previously pointed out, the method sequentially generates samples that are increasingly concentrated near the optimal solution set. In this regard, Fig. 4 shows the borehole locations obtained during four representative stages of the optimization process, namely, $j = 0$ (initial stage), $j = 3$ (intermediate stage), $j = 6$ (intermediate stage), and $j = 8$ (final stage). The initial boreholes are uniformly distributed over the search space and, thereafter, the effective support of the subsequent samples is consistently reduced. At the end of the procedure (see Fig. 4-d), the borehole positions densely populate a vicinity of the

foundation center which, according to Fig. 3, can be regarded as the optimal borehole position. That is, the proposed framework is able to identify the optimal borehole placement region in terms of a set of nearly-optimal soil sounding locations.

To gain additional insight into the optimization process, Fig. 5 shows the minimum and maximum values of the normalized standard deviation obtained during the different sampling stages. In accordance with the theoretical foundations of the search technique, it is noted that the effective support of $\bar{\sigma}_\zeta(\mathbf{b})$ tends to decrease as the number of stages increases. At the beginning of the procedure the normalized standard deviation values roughly lie between 0.6 and 1.0, whereas the final observed extrema are almost coincident. In fact, the last stage yields $\bar{\sigma}_\zeta(\mathbf{b}) \approx 0.6$. That is, the base (unconditioned) standard deviation of the foundation bearing capacity can be reduced in approximately 40% by placing a borehole near the region identified in Fig. 4-d. Furthermore, if a single solution is needed, the configuration that yields the smallest performance measure across all stages can be considered. In this case, the sample-based optimal borehole location is $\hat{\mathbf{b}}^* = [0.03, 0.34]^{\mathrm{T}}$ with $\bar{\sigma}_\zeta(\hat{\mathbf{b}}^*) = 0.59$.

One of the advantages of the proposed framework pertains to its ability to obtain non-trivial sensitivity information of the performance measure as a byproduct of the solution process. To illustrate this feature, consider the borehole locations obtained during stage $j = 6$ (see Fig. 4-c), which are associated with normalized standard deviations ranging from 0.59 to 0.60 (see Fig. 5). Since the support of these locations along the x direction is much narrower than along the y direction, the function $\bar{\sigma}_\zeta(\mathbf{b})$ seems to be much more sensitive to the x coordinate of the soil sounding than to its y coordinate near the foundation center. This outcome, which seems rather intuitive in this case and agrees with the behavior observed in Fig. 3, provides valuable insight for decision making. For example, more attention should be given to placing the soil sounding along the major axis of the foundation, whereas deviations of the borehole along the y axis are expected to have a limited impact on $\bar{\sigma}_\zeta(\mathbf{b})$ for this case.

The incorporation of soil soundings affects, in general, the probability distribution of the system bearing capacities. In this regard, Fig. 6 presents the normalized histograms of the bearing capacity for the unconditioned setting and for a single borehole placed at $\hat{\mathbf{b}}^* = [0.03, 0.34]^{\mathrm{T}}$. It is seen that placing the soil sounding at this position, which corresponds to the previously identified sample-based optimum, has a visible effect on the shape of the bearing capacity distribution. Specifically, the coefficient of variation is reduced from 0.28 to 0.16. Moreover, the corresponding expected

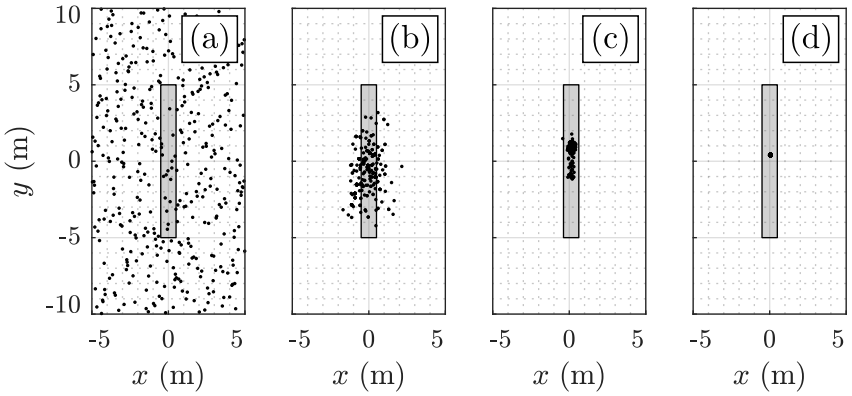

Figure 4: Borehole locations obtained at representative stages of the optimization process for $\theta_h = 5$ m. (a) Stage $j = 0$ (initial stage). (b) Stage $j = 3$. (c) Stage $j = 6$. (d) Stage $j = 8$ (final stage). Example 1.

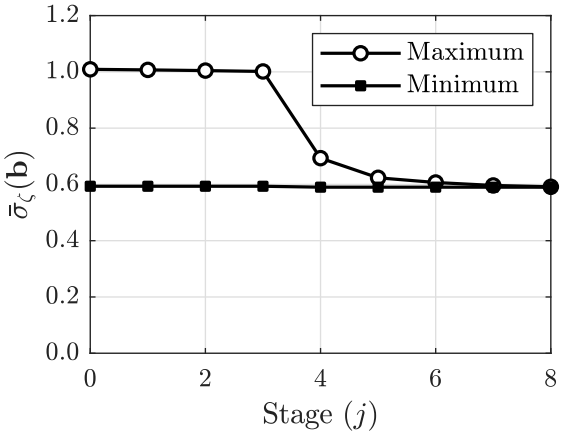

Figure 5: Maximum and minimum values of $\bar{\sigma}_\zeta(\mathbf{b})$ obtained during the different stages of the optimization process for $\theta_h = 5$ m. Example 1.

values are equal to 5.14×10^3 kN for the base condition case and to 5.28×10^3 kN when the borehole is taken into account. Considering the presentation in Section 3, it can thus be argued that placing the soil sounding at this location affects the standard deviation of the bearing capacity, σ_ζ, to a greater extent than the corresponding mean value, μ_ζ, for the case under consideration. Lastly, the results shown in Fig. 6 are obtained by the RFMM during the solution of Eq. (2) and, therefore, do not involve explicit assumptions for the distribution of the bearing capacity. That is, the proposed framework can provide additional information about the distribution of the system bearing capacities as a byproduct of the solution process.

The proposed framework can be employed to identify optimal configurations when multiple boreholes can be placed at the site of interest. In this regard, and assuming $\theta_h = 5$ m, the reference borehole locations obtained for $n_B = 1$, 2 and 3 available soil soundings are presented in Fig. 7. In all cases, the configurations seem to be symmetrical with respect to the foundation center. Moreover, the configurations identified for one and two boreholes agree with those reported in earlier

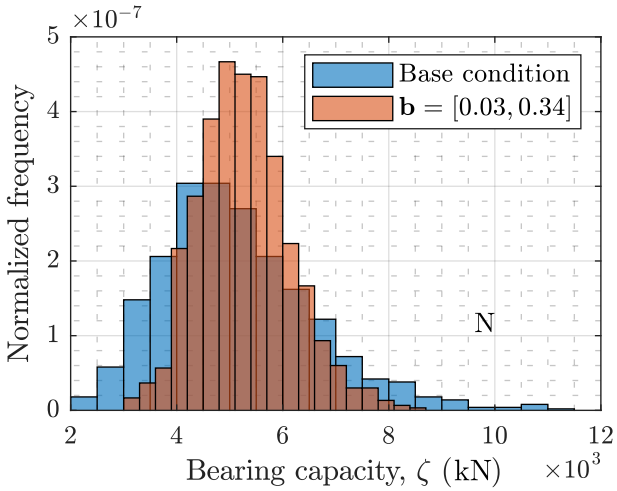

Figure 6: Histograms of the bearing capacity corresponding to the base condition and to the placement of a soil sounding at $\hat{\mathbf{b}}^* = [0.03, 0.34]^{\mathrm{T}}$ m for $\theta_h = 5$ m. Example 1.

studies [44, 45]. For reference purposes, the sample-based optimum of the normalized standard deviation corresponding to the three cases shown in Fig. 7 are reported in Table 1. These results indicate that increasing the number of boreholes tends to reduce the bearing capacity standard deviation, as expected. In this regard, placing a single borehole yields an optimal performance measure of 0.59, and placing two boreholes leads to $\bar{\sigma}_\zeta(\hat{\mathbf{b}}^*) = 0.15$. Thus, including a second borehole reduces the standard deviation of the bearing capacity in approximately 75%. Nevertheless, the results presented in the table suggest that incorporating a third soil sounding provides a negligible improvement of the optimal performance measure for the case under consideration.

Table 1: Sample-based optimum of the normalized standard deviation, $\bar{\sigma}_\zeta(\hat{\mathbf{b}}^*)$, corresponding to different numbers of boreholes, n_B, and $\theta_h = 5$ m. Example 1.

n_B	$\bar{\sigma}_\zeta(\hat{\mathbf{b}}^*)$
1	0.59
2	0.15
3	0.12

An assessment of the effect of the number of boreholes on the bearing capacity standard deviation can be performed by means of the proposed framework. Figure 8 shows, for different horizontal fluctuation scales, the optimal value of the normalized standard deviation in terms of the number of available soil soundings. Specifically, the values $\theta_h = 1$ m, 3 m, 5 m, and 20 m are considered. The figure indicates that, as expected, incorporating more soil soundings tends to reduce the bearing capacity standard deviation. However, points of diminishing returns can be identified in some cases. For instance, the results corresponding to $\theta_h = 20$ m show that, from a

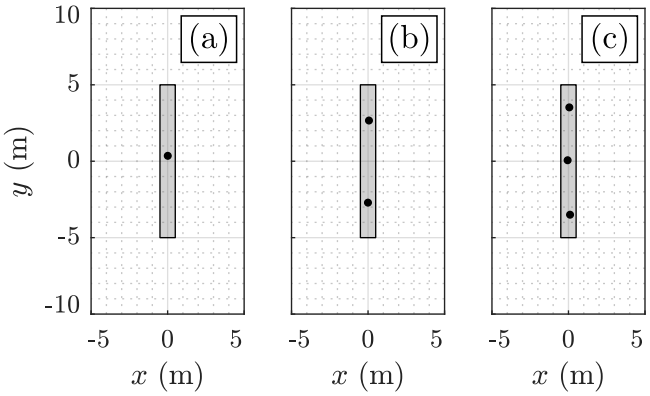

Figure 7: Target borehole locations obtained by the proposed framework. (a) One borehole. (b) Two boreholes. (c) Three boreholes. Example 1.

practical viewpoint, placing more than a single borehole will not yield further reductions in the bearing capacity standard deviation. Conversely, for $\theta_h = 1$ m it seems that considering more than $n_B = 5$ available soil soundings may lead to even smaller values for $\bar{\sigma}_\zeta$. Finally, greater reductions of the bearing capacity standard deviation are observed for longer fluctuation scales. In other words, soil sounding arrangements tends to decrease the variability of the bearing capacity estimates more effectively for soils with a stronger spatial correlation of its undrained shear strength. This insight, which seems reasonable from an engineering viewpoint, highlights the usefulness of the herein proposed framework to obtain non-trivial information for optimal soil sounding placement in the context of shallow foundation system design.

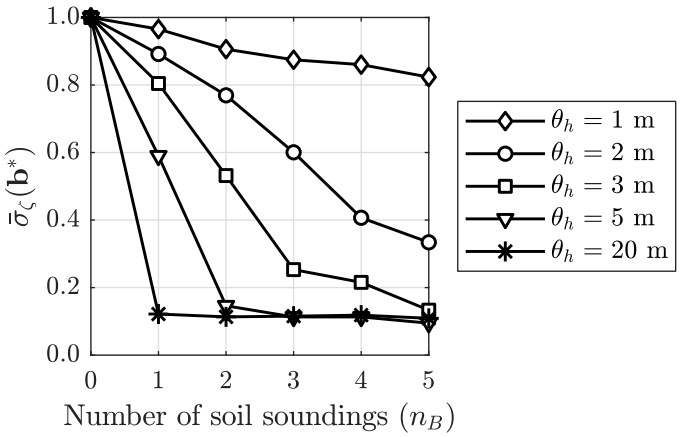

Figure 8: Optimal value of the normalized standard deviation in terms of the number of soil soundings for different values of the horizontal fluctuation scale, θ_h. Example 1.

6.2. Example 2

The second example under consideration addresses optimal soil sounding placement for the system of four square footings with size equal to 1 m shown in Fig. 2-b. Note that this system,

which is more complex than the one studied in Section 6.1, still allows identifying optimal borehole locations based on engineering judgment for some scenarios due to the regularity and symmetry of its configuration. Further, the two performance measures defined in Section 2.3 are adopted to identify optimal soil sounding locations.

First, the average normalized standard deviation defined in Eq. (3) is considered as the objective function of Eq. (2). For illustration purposes, the horizontal fluctuation scale is taken as $\theta_h = 5$ m. Then, the optimal borehole placement problem is solved for $n_B = 1, 2, 3$ and 4 available soil soundings. The corresponding target borehole locations obtained for the different values of n_B are represented in Fig. 9 in terms of the configurations obtained at the final stage of the optimization technique. When a single soil sounding is considered (see Fig. 9-a), the available soil sounding must be located near any footing center to minimize $\bar{\sigma}^{\text{avg}}(\mathbf{b})$. This finding agrees with previously reported results (see, e.g., [44]), which highlights the effectiveness of the proposed framework. Furthermore, Figs. 9-b, 9-c, and 9-d suggest that the optimal borehole locations lie near the centroids of the different footings when multiple soil soundings are available. Since placing a single borehole under the centroid of an isolated square footing yields the greatest reduction of its bearing capacity standard deviation [44], these results suggest that the choice of $\bar{\sigma}^{\text{avg}}(\mathbf{b})$ as performance measure leads to borehole locations that prioritize local variability reduction for the scenario under consideration.

Following the presentation in Section 2, the choice of the maximum normalized standard deviation as performance measure aims to identify borehole configurations that ensure a minimum level of information gain for all footings. To illustrate this feature, the proposed framework is implemented to identify borehole arrays that minimize $\bar{\sigma}^{\max}(\mathbf{b})$ for the foundation system of Fig. 2-b. Specifically, the horizontal fluctuation scale is taken as $\theta_h = 5$ m, and $n_B = 1, 2, 3$ and 4 available soil soundings are considered. Figure 10 shows the corresponding final designs obtained by the adopted search technique. In general, these configurations are quite different from those observed in Fig. 9. When a single soil sounding is available, its optimal location seems to lie near the center of the foundation system (see Fig. 10-a), which agrees with the findings reported in [44]. Furthermore, the borehole locations identified for $n_B = 2$ and $n_B = 3$ in Figs. 10-b and 10-c, respectively, lie along some of the symmetry axes of the foundation array. Finally, the results presented in Fig. 10-d indicate that the configurations that minimize $\bar{\sigma}^{\max}(\mathbf{b})$ for $n_B = 4$ are quite similar to those obtained when $\bar{\sigma}^{\text{avg}}(\mathbf{b})$ is adopted as performance measure. That is, when the same number

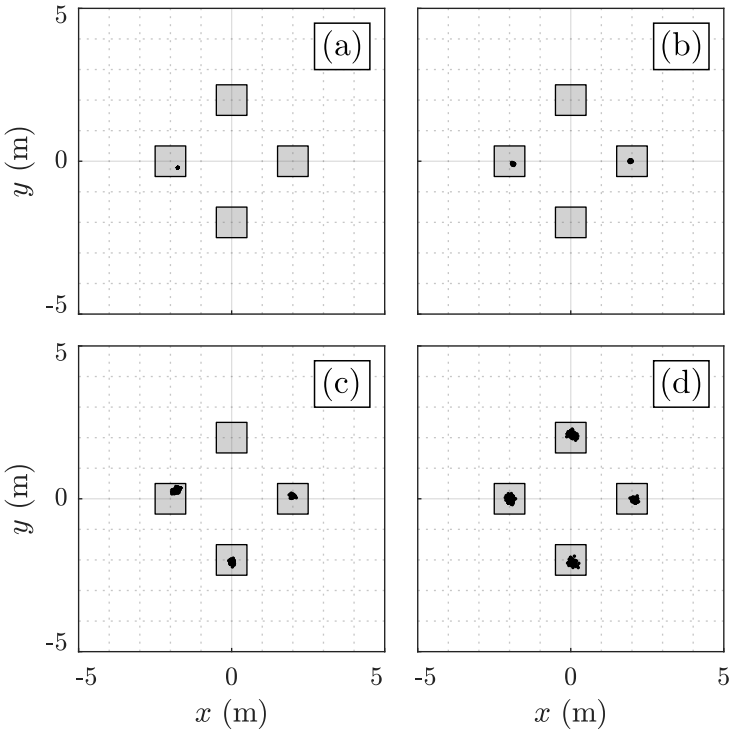

Figure 9: Final borehole locations obtained for $\bar{\sigma}^{\text{avg}}(\mathbf{b})$ and $\theta_h = 5$ m. (a) $n_B = 1$. (b) $n_B = 2$. (c) $n_B = 3$. (d) $n_B = 4$. Example 2.

of boreholes and footings is considered, the two performance measures presented in Section 2 lead to soil soundings placed relatively near the centers of the different footings in this case.

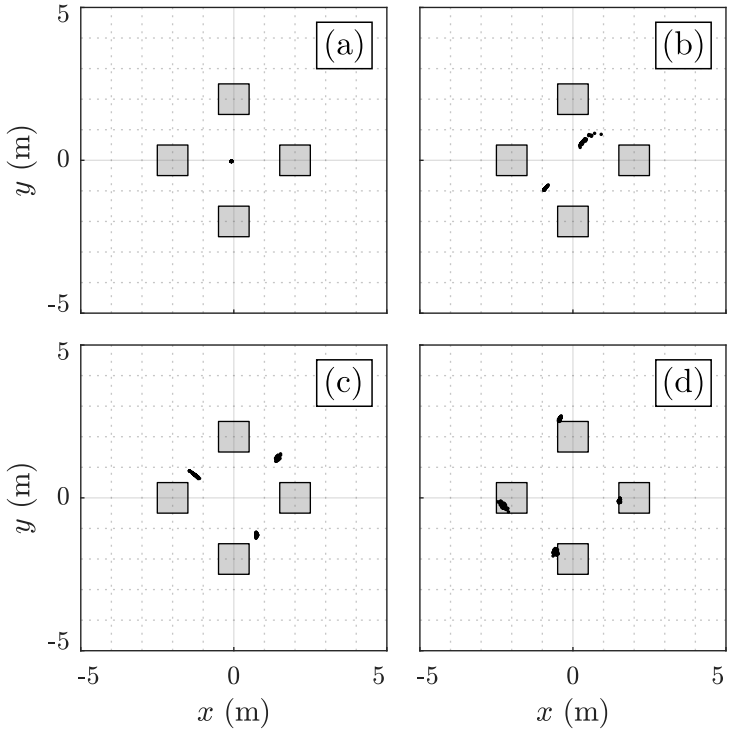

Figure 10: Final borehole locations obtained for $\bar{\sigma}^{\max}(\mathbf{b})$ and $\theta_h = 5$ m. (a) $n_B = 1$. (b) $n_B = 2$. (c) $n_B = 3$. (d) $n_B = 4$. Example 2.

The final configurations presented in Figs. 9 and 10 are obtained from the solution of Eq. (2), which presents several challenging characteristics for the case under consideration. Due to the symmetry of the foundation system, multiple borehole configurations can lead to very similar objective function values. For instance, when a single soil sounding is available, the corresponding borehole can be placed under the center of any foundation to achieve practically the same values for $\bar{\sigma}^{\text{avg}}(\mathbf{b})$ and $\bar{\sigma}^{\max}(\mathbf{b})$. Moreover, for a given configuration of boreholes with $n_B > 1$, any permutation of their locations will yield the same standard deviations of the different bearing capacities. Hence, the optimal borehole placement problem involves, in general, multiple solutions that minimize the performance measure under consideration. Furthermore, as already pointed out, the estimation of Eqs. (3) and (4) relies on stochastic simulation, which introduces additional challenges to the solution of Eq. (2). Despite the previous issues, validation calculations in the context of this example indicate that the proposed framework is able to identify optimal borehole configurations in a robust manner. Finally, it is noted that the borehole configurations presented in Figs. 9 and 10 can be viewed as candidate solutions according to different preferences of the analyst. While the results in Fig. 9 prioritize local usage of information, those in Fig. 10 yield a global reduction of the bearing capacity variability. In this regard, alternative performance measures can be directly implemented within the proposed framework as long as they are defined in terms of the second-order statistical moments of the different bearing capacities [46]. This highlights the flexibility of the proposed approach to aid the design of site investigation programs under diverse preferences of the decision maker.

One of the advantageous features of the proposed framework pertains to its ability to obtain nontrivial sensitivity information of the problem functions as a byproduct of the solution process. To illustrate this aspect, consider $n_B = 3$ available soil soundings and a horizontal fluctuation scale of $\theta_h = 20$ m. Further, the average normalized standard deviation, $\bar{\sigma}^{\text{avg}}(\mathbf{b})$, is adopted to identify optimal borehole locations. Then, Fig. 11 presents the minimum and maximum objective function values obtained during the different stages of the solution process. The results show that the effective support of $\bar{\sigma}^{\text{avg}}(\mathbf{b})$ tends to decrease as the number of stages increases. At the final stage, the objective function values range from 0.106 to 0.107. Moreover, previous stages also yield a relatively narrow effective support for $\bar{\sigma}^{\text{avg}}(\mathbf{b})$. Specifically, the objective function values obtained at stage $j = 5$ range from 0.106 to 0.110 and, therefore, the corresponding borehole configurations can be regarded as equivalent from a practical viewpoint.

To gain further insight into the previous results, Fig. 12 presents the soil sounding arrays obtained during three representative stages of the solution process, namely, $j = 0$ (initial stage), $j = 5$ (intermediate stage), and $j = 10$ (final stage). The final borehole configurations constitute a set of nearly optimal solutions and, therefore, characterize target locations for the available soil soundings. Nevertheless, the locations obtained at stage $j = 5$ (see Fig. 12-b) are equivalent from an objective function viewpoint (see Fig. 11) to the final set of designs shown in Fig. 12-c. Therefore, it can be argued that relatively small deviations of the different boreholes with respect to their identified target locations are not expected to have a significant impact on $\bar{\sigma}^{\text{avg}}(\mathbf{b})$. These results seem reasonable given the relatively strong spatial correlation of the undrained shear strength for the case under consideration. Hence, nontrivial information about the interaction between the bearing capacity standard deviations and the borehole locations can be obtained by the proposed framework for this example.

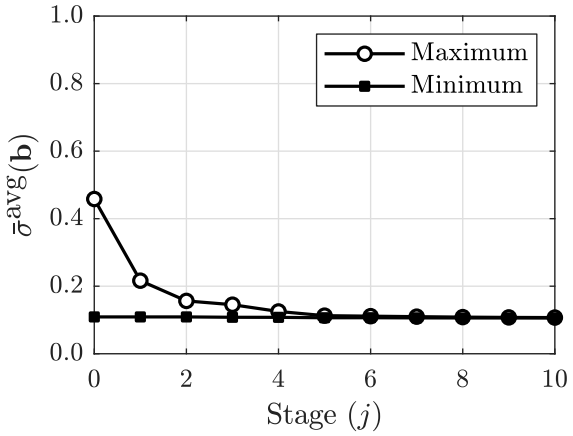

Figure 11: Maximum and minimum values of $\bar{\sigma}^{\text{avg}}(\mathbf{b})$ obtained during the solution process for $n_B = 3$ and $\theta_h = 20$ m. Example 2.

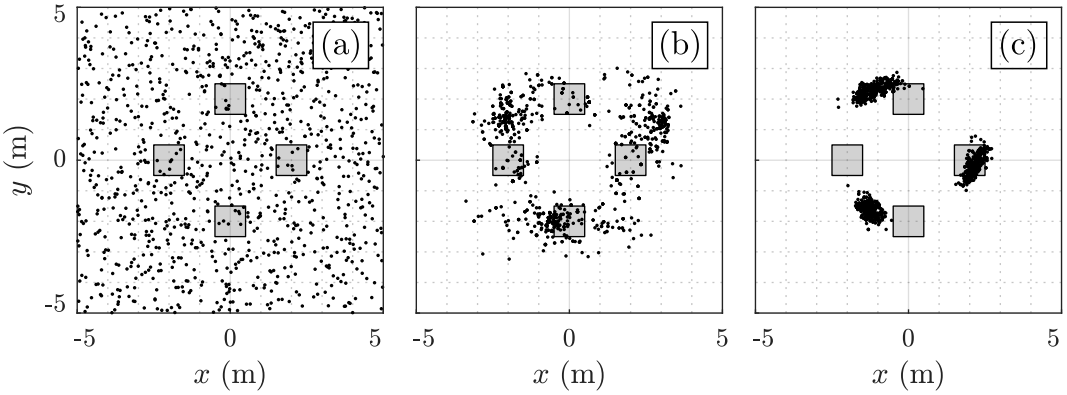

Figure 12: Borehole configurations generated during representative stages of the solution process for $n_B = 3$, $\theta_h = 20$ m, and $\bar{\sigma}^{\text{avg}}(\mathbf{b})$. (a) $j = 0$ (initial stage). (b) $j = 5$ (intermediate stage). (c) $j = 10$ (final stage). Example 2.

6.3. Example 3

To assess the capabilities of the proposed framework in a more general scenario, the arrangement of four foundations presented in Fig. 2-c is considered in the third example. The system is composed of one central foundation of 1 m width and 6 m length, two square footings of size equal to 1 m located on one side, and one foundation of 1 m width and 8 m length on the other side. Since the foundations are asymmetrically placed and have different sizes, it is arguably not straightforward to determine target locations for available boreholes based solely on engineering judgment. In this context, the use of supportive analysis tools, such as the herein proposed framework, can be rather helpful.

Assuming a total of $n_B = 3$ soil soundings and a horizontal fluctuation scale of $\theta_h = 5$ m, the two performance measures defined in Eqs. (3) and (4) are employed to identify target borehole locations. The corresponding optimal configurations associated with both objective functions are shown in Fig. 13. According to these results, it it seen that $\bar{\sigma}^{\text{avg}}(\mathbf{b})$ (see Fig. 13-a) leads to soil soundings placed near the centers of the three smallest footings, while no soil soundings are placed under the rightmost foundation. Alternatively, choosing $\bar{\sigma}^{\max}(\mathbf{b})$ as objective function yields a fairly different optimal configuration, as shown in Fig. 13-b. Notably, one soil sounding is placed between the two squared footings, while the remaining boreholes are located near the remaining foundations. To obtain further insight, Table 2 reports the normalized standard deviations of the foundation bearing capacities corresponding to such optimal configurations. The results presented in the table agree with some of the ideas discussed in [46]. On the one hand, the choice of $\bar{\sigma}^{\text{avg}}(\mathbf{b})$ as performance measure tends to privilege local gain of information at the expense of not reducing the standard deviation of the rightmost foundation. On the other hand, $\bar{\sigma}^{\max}(\mathbf{b})$ tends to ensure global gain of information, although the individual reductions in some of the standard deviations may be smaller than those achieved with the use of $\bar{\sigma}^{\text{avg}}(\mathbf{b})$. It is noted that the soil sounding locations shown in Fig. 13 are not straightforward to determine a priori, which highlights the applicability of the proposed framework.

According to the discussion in Section 4, the optimization technique adopted for the solution of Eq. (2) involves the evaluation of the objective function at a number of designs during each stage. This requires the repeated estimation of the bearing capacity standard deviations by means of the RFMM, which can in turn lead to considerable computational efforts. To address this issue, an adaptive metamodel strategy based on kriging interpolants is implemented to approximate the

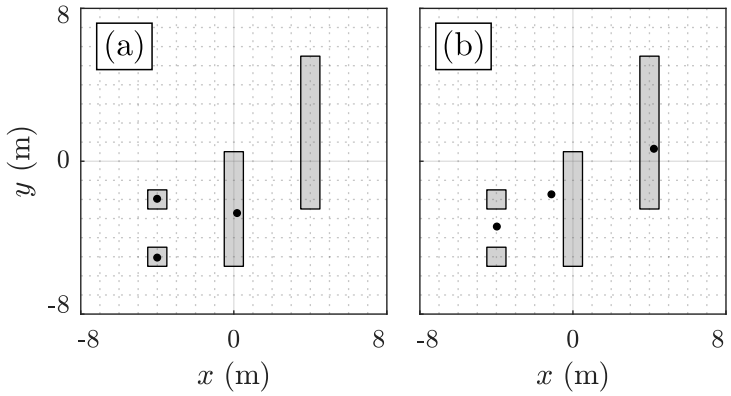

Figure 13: Target borehole locations obtained for $n_B = 3$, $\theta_h = 5$ m, and different performance measures. (a) $\bar{\sigma}^{\text{avg}}(\mathbf{b})$. (b) $\bar{\sigma}^{\max}(\mathbf{b})$. Example 3.

Table 2: Normalized standard deviations of the foundation bearing capacities corresponding the borehole configurations in Fig. 13. Example 3.

Foundation	Configuration in Fig. 13-a	Configuration in Fig. 13-b
Leftmost-lower	0.10	0.58
Leftmost-upper	0.09	0.58
Center	0.38	0.56
Rightmost	1.00	0.58

standard deviations (see Section 5.2). For illustration purposes, Fig. 14 shows the acceptance rate of the kriging predictions obtained during the different stages of the solution process to determine the optimal configuration in Fig. 13-b. Since the initial set of designs (stage $j = 0$) is directly evaluated using the RFMM to initialize the database of support points, the adaptive metamodel strategy is employed only from stage $j = 1$ until the final stage ($j = 11$). The figure indicates that the acceptance rate is fairly high. In fact, the average acceptance rate from stage $j = 1$ to stage $j = 11$ is equal to 94%. Furthermore, taking into account that the initial set of designs (stage $j = 0$) and those incorporated to the database of support points in stages $j = 1, 2, \ldots, 11$ are evaluated using the RFMM, the number of direct evaluations of the objective function represents approximately 14% of the total number of designs generated throughout the entire optimization process. In general, a similar behavior is observed for the different cases studied in this contribution, with average acceptance rates of at least 80%. This highlights the effectiveness of the adopted metamodel strategy to reduce the overall computational costs of the solution procedure. Certainly, alternative surrogate strategies can be also considered to enhance the numerical efficiency of the herein proposed framework.

As previously pointed out, geotechnical engineering practice commonly faces lack of statistical

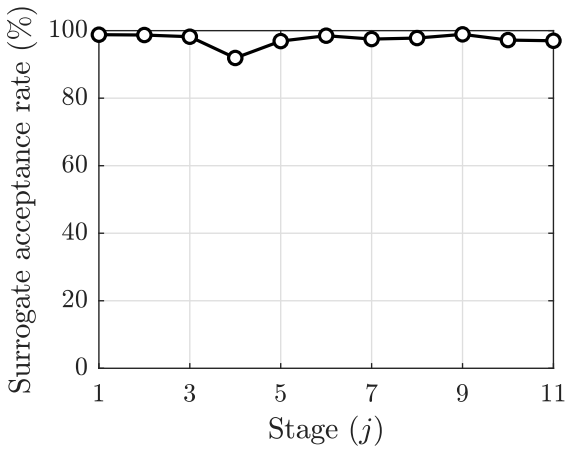

Figure 14: Metamodel acceptance rate during the different stages of the solution process. Example 3.

information about mechanical soil properties. In this context, the herein proposed framework can be employed to assess the sensitivity of final designs with respect to, e.g., the fluctuation scales of the undrained shear strength. To illustrate this feature, and considering $n_B = 3$ and $\theta_h = 5$ m, optimal borehole locations are identified in terms of $\bar{\sigma}^{\text{avg}}(\mathbf{b})$ for different values of the vertical fluctuation scale, namely, $\theta_v = 0.5$ m, 1.0 m, and 2.0 m. Such configurations are presented in Fig. 15. It can be seen that the results obtained for $\theta_v = 0.5$ m and $\theta_v = 1.0$ m are very similar between each other, i.e., the boreholes lie near the centers of the leftmost and central foundations in both cases. Instead, different results are observed for $\theta_v = 2$ m, where Fig. 15-c indicates that the average normalized standard deviation can be minimized by placing the soil soundings near the centers of the leftmost and rightmost foundations. In this regard, it is noted that independent runs of the search technique also identify target configurations that are similar to, e.g., the one presented in Fig. 15-a. However, such borehole arrangements yield objective function values that are very similar to the one obtained with the configuration in Fig. 15-c. Thus, it can be stated that, from a practical viewpoint, $\theta_v = 2.0$ m yields multiple optima in terms of the obtained target locations. On the contrary, this issue is not observed for shorter vertical fluctuation scales, namely, $\theta_v = 0.5$ m and $\theta_v = 1.0$ m. In these cases, independent optimization runs consistently identified target locations that are very similar to those in Fig. 15-a and 15-b. This suggests that the vertical fluctuation scale, θ_v, can have an impact on optimal borehole configurations due to its effect on the overall spatial correlation of the undrained shear strength. Such effect is expected to depend on the particular characteristics of the system under consideration, including the horizontal fluctuation scale, foundation sizes, and distances between footings. Lastly, it is noted that similar analyses can be performed, for instance, in terms of alternative parameters involved in the characterization

of mechanical soil properties.

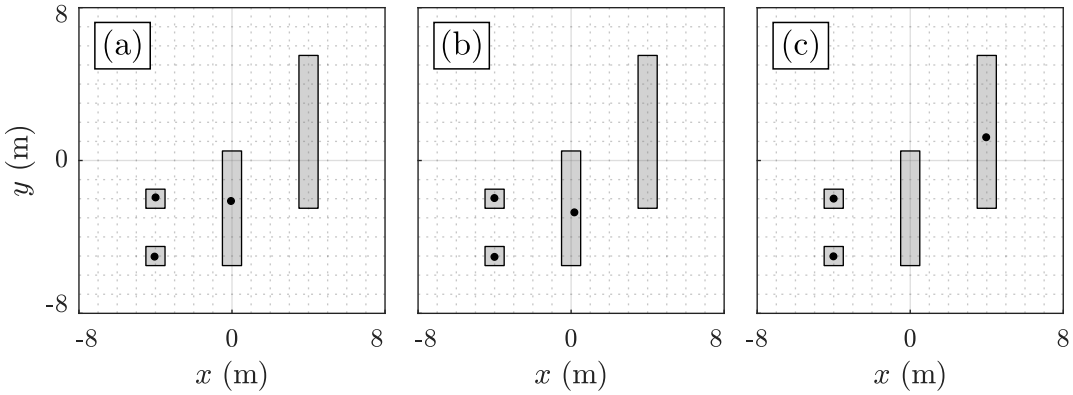

Figure 15: Target borehole locations, in terms of $\bar{\sigma}^{\text{avg}}(\mathbf{b})$, obtained for $n_B = 3$ soil soundings and different vertical fluctuation scales. (a) $\theta_v = 0.5$ m. (b) $\theta_v = 1.0$ m. (c) $\theta_v = 2.0$ m. Example 3.

One relevant aspect of site investigation programs pertains to the choice of an appropriate number of soil soundings. As discussed in Section 6.1, the herein proposed framework can be employed to explore the tradeoff between the available number of boreholes and the corresponding optimal values of the chosen performance measure. Figure 16 presents the optimal value of $\bar{\sigma}^{\max}(\mathbf{b})$, in terms of the number of soil soundings, for different horizontal fluctuation scales. In general, the optimal values obtained for shorter fluctuation scales and relatively few soil soundings are close to one. This can be regarded as an indication that such a number of boreholes cannot yield a global reduction of the bearing capacity standard deviations. Hence, more soil soundings must be incorporated or, alternatively, the aim of the site investigation program design may need to be changed. Further, the figure indicates that, for longer fluctuation scales, less boreholes are required to achieve a certain reduction of the adopted performance measure. Indicatively, for $\theta_h = 10$ m including $n_B = 2$ soil soundings yields an optimal value of $\bar{\sigma}_{\zeta}^{\max}(\mathbf{b}^*) \approx 0.39$, whereas the consideration of $n_B = 5$ boreholes in the case $\theta_h = 5$ m leads to $\bar{\sigma}_{\zeta}^{\max}(\mathbf{b}^*) \approx 0.48$. In other words, a greater relative reduction of the bearing capacities can obtained with less boreholes when longer fluctuation scales are considered. Moreover, for relatively short fluctuation scales (say, $\theta_h \leqslant 2.0$ m) it seems that the bearing capacity standard deviations cannot be significantly reduced for the values of n_B under consideration. For instance, in the case $\theta_h = 2$ m, the optimal objective function values for $n_B = 1$ and $n_B = 5$ are 0.99 and 0.87, respectively. This represents a relative improvement of roughly 12% which, for instance, may not be sufficient to justify the increased investment associated with the implementation of four additional soil soundings. A similar type of analysis can be conducted in terms of, e.g., the average normalized standard deviation, $\bar{\sigma}^{\text{avg}}(\mathbf{b})$.

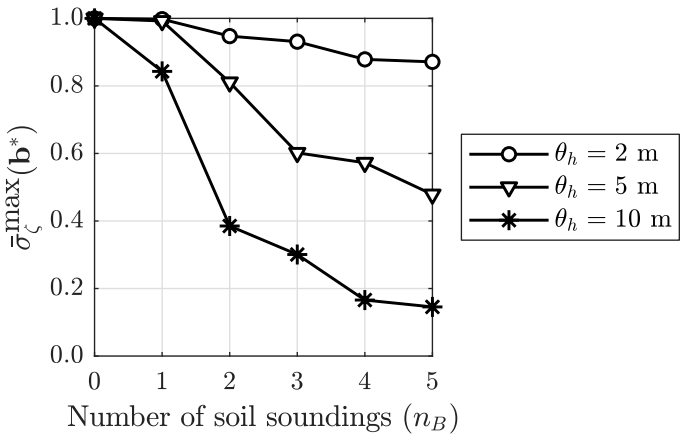

Figure 16: Optimal value of the maximum normalized standard deviation in terms of the number of soil soundings for different values of the horizontal fluctuation scale, θ_h. Example 3.

Overall, the results presented in this example illustrate the ability of the method to obtain non-trivial insight for decision making considering general foundation layouts such as the one presented in Fig. 2-c. In this regard, the approach proposed in this contribution furnishes analysis tools to assess not only the effect of the number of sensors on optimal bearing capacity standard deviations, but also the sensitivity of final designs with respect to the probabilistic characterization of mechanical soil properties. The latter feature is particularly valuable when limited prior knowledge about the statistical properties of the supporting soil is available, which is a rather common situation in geotechnical engineering practice. Thus, it can be argued that the herein proposed framework shows potentiality to be implemented as a supportive tool for the design of site investigation programs.

7. Conclusions

This contribution has presented a framework to address optimal soil sounding placement problems in the context of shallow foundation design under spatially variable, undrained soil conditions. To identify optimal borehole configurations, a suitable optimization problem is formulated. The corresponding objective function quantifies the reduction, with respect to the base scenario, of the bearing capacity standard deviations due to the presence of soil soundings. Two performance measures are considered, namely, the average and maximum normalized standard deviation of the system bearing capacities. By resorting to the random failure mechanism method (RFMM), these measures are estimated in a numerically tractable fashion while fully accounting for the spatial variability of undrained shear strength. In addition, a stochastic search technique that relies on an

equivalent sampling problem is adopted as optimization method, thereby retrieving valuable sensitivity information as a byproduct of the solution process. Moreover, specialized implementation strategies are discussed to enhance the numerical efficiency of the proposed approach.

The applicability and advantages of the herein proposed framework are demonstrated in three examples involving different foundation layouts. These include a single rectangular foundation, a symmetrical arrangement of four identical squared footings, and a non-symmetrical system involving four foundations of different sizes. For each example, different scenarios are studied in terms of the number of available soil soundings and the fluctuation scales of the underlying random field. Despite the challenging characteristics of the associated optimization problems, the approach allows identifying target locations for the available soil soundings in an effective manner. Such locations are obtained in terms of a set of nearly-optimal borehole configurations rather than a single final solution, which enables additional flexibility for decision making. Considering the inherent variability arising in the estimation of bearing capacity standard deviations, this strategy can be regarded as a prudent and appropriate choice for optimal soil sounding placement. Furthermore, another advantage of the proposed framework pertains to its ability to obtain non-trivial sensitivity information about the effect of borehole locations into bearing capacities. Specifically, the soil sounding arrays obtained throughout the different optimization stages, and the related bearing capacity histograms, provide valuable insight about the problem at hand. Finally, additional types of analyses for the design of site investigation programs can be carried out by the approach. Notably, the sensitivity of final designs with respect to fluctuation scales and the effect of the number of soil soundings on bearing capacity variability can be assessed in a unified formulation by virtue of the proposed framework, whereby a thorough assessment of potential design conditions can be developed. This feature is particularly valuable not only due to the usual unavailability of prior information about soil properties, but also to the typically high investment levels that soil sounding techniques require in their implementation. Overall, the above discussion and the numerical results presented in this contribution suggest that the herein proposed framework can be potentially adopted as a supportive tool to assist the design of site investigation programs in a class of geotechnical engineering problems.

Future research efforts consider the extension of the proposed approach to additional classes of shallow foundation systems, such as those involving, e.g., cohesive-frictional and ponderable soils, smooth-based foundations, mechanical interaction between footings, and non-stationary random

fields for the characterization of soil properties. Besides, the proposed framework could also be implemented in a comprehensive study for typical foundation layouts which, based on theoretical findings, may provide general guidelines for soil sounding placement in practical situations. Some of these topics are currently under consideration.

Acknowledgments

This research is partially supported by the Polish National Agency for Academic Exchange under the Bekker NAWA Programme, Grant No. BPN/BEK/2021/1/00068, which funded the postdoctoral stay of the second author at the Institute for Risk and Reliability, Leibniz Universität Hannover. In addition, this paper is based upon work partially funded by ANID (National Agency for Research and Development, Chile) under FONDECYT No. 1200087. These supports are gratefully acknowledged by the authors.

A. Kinematic method of limit analysis

For simplicity, the bearing capacity of a given foundation is denoted in this appendix by ζ, the dissipation regions of its failure mechanism by R_i, $i = 1, \ldots, 30$, and the corresponding averaged undrained shear strengths by $\bar{c}_{u,R_i}$, $i = 1, \ldots, 30$. The reference points shown in Fig. 1 are related to the different dissipation regions according to Table 3. In this regard, R_i, $i = 1, \ldots, 4$, correspond to rectangular regions; R_i, $i = 5, \ldots, 20$, to triangular regions; R_{21} and R_{22} to sections of solid cylinders; and R_i, $i = 23, \ldots, 30$, to conical regions.

Table 3: Dissipation regions of a single failure mechanism in terms of the reference points shown in Fig. 1.

Region	Points	Region	Points	Region	Points
R_1	ABFE	R_{11}	UEP	R_{21}	ABC-EFG
R_2	DCHG	R_{12}	USR	R_{22}	AMN-EPR
R_3	AMEP	R_{13}	IAJ	R_{23}	EFG-W
R_4	NORS	R_{14}	TAJ	R_{24}	ABC-I
R_5	ABI	R_{15}	IKL	R_{25}	EPR-U
R_6	ICD	R_{16}	TKL	R_{26}	AMN-T
R_7	EFW	R_{17}	WEZ	R_{27}	AKJ-I
R_8	GWH	R_{18}	WXY	R_{28}	AKJ-T
R_9	TAM	R_{19}	UEZ	R_{29}	EYZ-W
R_{10}	TON	R_{20}	UXY	R_{30}	EYZ-U

The ultimate load associated with the failure mechanism shown in Fig. 1, for given values of $\bar{c}_{u,i}$, $i = 1, \ldots, 30$, is denoted by $\tilde{\zeta}$ and expressed as

$$\tilde{\zeta} = \tilde{\zeta}_{(1)} + \tilde{\zeta}_{(2)} + \tilde{\zeta}_{(3)} + \tilde{\zeta}_{(4)} \tag{10}$$

with

$$\tilde{\zeta}_{(1)} = b_2(a - (d_1 + d_2))m_1 + 0.5b_2 d_1 n_1 m_2 + 0.5b_2 d_2 n_2 m_3 \tag{11}$$

$$\tilde{\zeta}_{(2)} = b_1(a - (d_1 + d_2))m_4 + 0.5b_1 d_1 n_3 m_5 + 0.5b_1 d_2 n_4 m_6 \tag{12}$$

$$\tilde{\zeta}_{(3)} = 0.5b_1 d_1 n_5 m_7 + 0.5b_2 d_1 n_6 m_8 \tag{13}$$

$$\tilde{\zeta}_{(4)} = 0.5b_1 d_2 n_7 m_9 + 0.5b_2 d_2 n_8 m_{10} \tag{14}$$

where the coefficients m_i, $i = 1, \ldots, 10$, and n_i, $i = 1, \ldots, 8$, are given in Tables 4 and 5, respectively.

The ultimate bearing load of any admissible failure mechanism provides an upper bound to the bearing capacity, that is, $\tilde{\zeta} \geqslant \zeta$. Then, the expression in Eq. (10) is minimized in terms of the geometrical parameters α_j, β_j, $j = 1, \ldots, 4$, d_1, d_2, b_1, to determine the best upper bound to the bearing capacity, i.e., $\tilde{\zeta}^* = \min \tilde{\zeta}$. Any suitable optimization technique can be adopted to this end [39]. Finally, the foundation bearing capacity is evaluated as $\zeta = \tilde{\zeta}^*$.

Table 4: Coefficients m_i, $i = 1, \ldots, 10$, involved in Eqs. (10) to (14).

Coefficient	Expression
m_1	$\bar{c}_{u,R_2} \cot \alpha_2 + 2\bar{c}_{u,R_{21}}(\alpha_2 + \beta_2) + \bar{c}_{u,R_1} \cot \beta_2$
m_2	$\bar{c}_{u,R_6} \cot \alpha_2 + 2\bar{c}_{u,R_{24}}(\alpha_2 + \beta_2) + \bar{c}_{u,R_5} \cot \beta_2$
m_3	$\bar{c}_{u,R_8} \cot \alpha_2 + 2\bar{c}_{u,R_{23}}(\alpha_2 + \beta_2) + \bar{c}_{u,R_7} \cot \beta_2$
m_4	$\bar{c}_{u,R_4} \cot \alpha_3 + 2\bar{c}_{u,R_{22}}(\alpha_3 + \beta_3) + \bar{c}_{u,R_3} \cot \beta_3$
m_5	$\bar{c}_{u,R_{10}} \cot \alpha_3 + 2\bar{c}_{u,R_{26}}(\alpha_3 + \beta_3) + \bar{c}_{u,R_9} \cot \beta_3$
m_6	$\bar{c}_{u,R_{12}} \cot \alpha_3 + 2\bar{c}_{u,R_{25}}(\alpha_3 + \beta_3) + \bar{c}_{u,R_{11}} \cot \beta_3$
m_7	$\bar{c}_{u,R_{16}} \cot \alpha_1 + 2\bar{c}_{u,R_{28}}(\alpha_1 + \beta_1) + \bar{c}_{u,R_{14}} \cot \beta_1$
m_8	$\bar{c}_{u,R_{15}} \cot \alpha_1 + 2\bar{c}_{u,R_{27}}(\alpha_1 + \beta_1) + \bar{c}_{u,R_{13}} \cot \beta_1$
m_9	$\bar{c}_{u,R_{20}} \cot \alpha_4 + 2\bar{c}_{u,R_{30}}(\alpha_4 + \beta_4) + \bar{c}_{u,R_{19}} \cot \beta_4$
m_{10}	$\bar{c}_{u,R_{18}} \cot \alpha_4 + 2\bar{c}_{u,R_{29}}(\alpha_4 + \beta_4) + \bar{c}_{u,R_{17}} \cot \beta_4$

Table 5: Coefficients n_i, $i = 1, \ldots, 8$, involved in Eqs. (10) to (14).

Coefficient	Expression
n_1	$\sqrt{1 + (b_2/d_1 \sin \beta_2)^2}$
n_2	$\sqrt{1 + (b_2/d_2 \sin \beta_2)^2}$
n_3	$\sqrt{1 + (b_1/d_1 \sin \beta_3)^2}$
n_4	$\sqrt{1 + (b_1/d_2 \sin \beta_3)^2}$
n_5	$\sqrt{1 + (d_1/b_1 \sin \beta_1)^2}$
n_6	$\sqrt{1 + (d_1/b_2 \sin \beta_1)^2}$
n_7	$\sqrt{1 + (d_2/b_1 \sin \beta_4)^2}$
n_8	$\sqrt{1 + (d_2/b_2 \sin \beta_4)^2}$

References

[1] R. B. Peck, Advantages and limitations of the observational method in applied soil mechanics, Géotechnique 19 (2) (1969) 171–187. doi:10.1680/geot.1969.19.2.171.

[2] R. D. Andrus, K. H. Stokoe II, Liquefaction resistance of soils from shear-wave velocity, Journal of Geotechnical and Geoenvironmental Engineering 126 (11) (2000) 1015–1025. doi:10.1061/(asce)1090-0241(2000)126:11(1015).

[3] R. L. Parsons, J. D. Frost, Evaluating site investigation quality using GIS and geostatistics, Journal of Geotechnical and Geoenvironmental Engineering 128 (6) (2002) 451–461. doi:10.1061/(asce)1090-0241(2002)128:6(451).

[4] W. Liu, A. Li, W. Fang, P. E. D. Love, T. Hartmann, H. Luo, A hybrid data-driven model for geotechnical reliability analysis, Reliability Engineering & System Safety 231 (2023) 108985. doi:10.1016/j.ress.2022.108985.

[5] T. Lunne, J. J. M. Powell, P. K. Robertson, Cone penetration testing in geotechnical practice, CRC Press, 2002. doi:10.1201/9781482295047.

[6] G. Vessia, D. D. Curzio, A. Castrignanò, Modeling 3D soil lithotypes variability through geostatistical data fusion of CPT parameters, Science of The Total Environment 698 (2020) 134340. doi:10.1016/j.scitotenv.2019.134340.

[7] J. Konkol, K. Międlarz, L. Bałachowski, Geotechnical characterization of soft soil deposits in Northern Poland, Engineering Geology 259 (2019) 105187. doi:10.1016/j.enggeo.2019.105187.

[8] P. K. Robertson, D. J. Woeller, W. D. L. Finn, Seismic cone penetration test for evaluating liquefaction potential under cyclic loading, Canadian Geotechnical Journal 29 (4) (1992) 686–695. doi:10.1139/t92-075.

[9] P. K. Robertson, Cone penetration test (CPT)-based soil behaviour type (SBT) classification system — an update, Canadian Geotechnical Journal 53 (12) (2016) 1910–1927. doi:10.1139/cgj-2016-0044.

[10] K. Sudha, M. Israil, S. Mittal, J. Rai, Soil characterization using electrical resistivity tomography and geotechnical investigations, Journal of Applied Geophysics 67 (1) (2009) 74–79. doi:10.1016/j.jappgeo.2008.09.012.

[11] Y. Wang, Z. Cao, Probabilistic characterization of Young's modulus of soil using equivalent samples, Engineering Geology 159 (2013) 106–118. doi:10.1016/j.enggeo.2013.03.017.

[12] K.-K. Phoon, F. H. Kulhawy, Characterization of geotechnical variability, Canadian Geotechnical Journal 36 (4) (1999) 612–624. doi:10.1139/t99-038.

[13] G. A. Fenton, D. V. Griffiths, Risk assessment in geotechnical engineering, John Wiley & Sons, New York, 2008.

[14] V. Ferreira, T. Panagopoulos, R. Andrade, C. Guerrero, L. Loures, Spatial variability of soil properties and soil erodibility in the Alqueva reservoir watershed, Solid Earth 6 (2) (2015) 383–392. doi:10.5194/se-6-383-2015.

[15] O. E. Oluwatuyi, K. Ng, S. S. Wulff, Improved resistance prediction and reliability for bridge pile foundation in shales through optimal site investigation plans, Reliability Engineering & System Safety 239 (2023) 109476. doi:10.1016/j.ress.2023.109476.

[16] C. Li, Y. Diao, H.-N. Li, H. Pan, R. Ma, Q. Han, Y. Xing, Seismic performance assessment of a sea-crossing cable-stayed bridge system considering soil spatial variability, Reliability Engineering & System Safety 235 (2023) 109210. doi:10.1016/j.ress.2023.109210.

[17] W. Gong, Y.-M. Tien, C. H. Juang, J. R. Martin, Z. Luo, Optimization of site investigation program for improved statistical characterization of geotechnical property based on random field theory, Bulletin of Engineering Geology and the Environment 76 (3) (2016) 1021–1035. doi:10.1007/s10064-016-0869-3.

[18] L. Huang, S. Huang, Z. Lai, On the optimization of site investigation programs using centroidal Voronoi tessellation and random field theory, Computers and Geotechnics 118 (2020) 103331. doi:10.1016/j.compgeo.2019.103331.

[19] M. P. Crisp, M. B. Jaksa, Y. L. Kuo, Characterising site investigation performance in multiple-layer soils and soil lenses, Georisk: Assessment and Management of Risk for Engineered Systems and Geohazards 15 (3) (2020) 196–208. doi:10.1080/17499518.2020.1806332.

[20] Z. Guan, Y. Wang, T. Zhao, Adaptive sampling strategy for characterizing spatial distribution of soil liquefaction potential using cone penetration test, Journal of Rock Mechanics and Geotechnical Engineering 14 (4) (2022) 1221–1231. doi:10.1016/j.jrmge.2022.01.011.

[21] D.-Q. Li, X.-H. Qi, Z.-J. Cao, X.-S. Tang, K.-K. Phoon, C.-B. Zhou, Evaluating slope stability uncertainty using coupled Markov chain, Computers and Geotechnics 73 (2016) 72–82. doi:10.1016/j.compgeo.2015.11.021.

[22] Y. Li, C. Qian, K. Liu, Sampling efficiency in spatially varying soils for slope stability assessment, Advances in Civil Engineering 2019 (2019) 1–15. doi:10.1155/2019/8267601.

[23] Y. J. Li, M. A. Hicks, P. J. Vardon, Uncertainty reduction and sampling efficiency in slope designs using 3D conditional random fields, Computers and Geotechnics 79 (2016) 159–172. doi:10.1016/j.compgeo.2016.05.027.

[24] S.-H. Jiang, I. Papaioannou, D. Straub, Optimization of site-exploration programs for slope-reliability assessment, ASCE-ASME Journal of Risk and Uncertainty in Engineering Systems, Part A: Civil Engineering 6 (1) (2020) 04020004. doi:10.1061/ajrua6.0001042.

[25] R. Yang, J. Huang, D. V. Griffiths, Optimal geotechnical site investigations for slope reliability assessment considering measurement errors, Engineering Geology 297 (2022) 106497. doi:10.1016/j.enggeo.2021.106497.

[26] L. Zhang, L. Wang, Optimization of site investigation program for reliability assessment of undrained slope using Spearman rank correlation coefficient, Computers and Geotechnics 155 (2023) 105208. doi:10.1016/j.compgeo.2022.105208.

[27] J. S. Goldsworthy, M. B. Jaksa, G. A. Fenton, W. S. Kaggwa, V. Griffiths, H. G. Poulos, Effect of sample location on the reliability based design of pad foundations, Georisk: Assessment and Management of Risk for Engineered Systems and Geohazards 1 (3) (2007) 155–166. doi:10.1080/17499510701697377.

[28] J.-Z. Hu, J.-G. Zheng, J. Zhang, H.-W. Huang, Bayesian framework for assessing effectiveness of geotechnical site investigation programs, ASCE-ASME Journal of Risk and Uncertainty in Engineering Systems, Part A: Civil Engineering 9 (1) (2023) 04022054. doi:10.1061/ajrua6.0001278.

[29] J. Pieczyńska-Kozłowska, G. Vessia, Spatially variable soils affecting geotechnical strip foundation design, Journal of Rock Mechanics and Geotechnical Engineering 14 (3) (2022) 886–895. doi:10.1016/j.jrmge.2021.10.010.

[30] M. Kawa, W. Puła, 3D bearing capacity probabilistic analyses of footings on spatially variable c-ϕ soil, Acta Geotechnica 15 (6) (2020) 1453–1466. doi:10.1007/s11440-019-00853-3.

[31] J. T. Simões, L. C. Neves, A. N. Antão, N. M. C. Guerra, Probabilistic analysis of bearing capacity of shallow foundations using three-dimensional limit analyses, International Journal of Computational Methods 11 (02) (2014) 1342008. doi:10.1142/s0219876213420085.

[32] C. C. M. Bolaños, J. E. Hurtado, Effects of soil test variability in the bearing capacity of shallow foundations, Transportation Infrastructure Geotechnology 9 (6) (2022) 854–873. doi:10.1007/s40515-021-00201-7.

[33] T. Al-Bittar, A.-H. Soubra, J. Thajeel, Kriging-based reliability analysis of strip footings resting on spatially varying soils, Journal of Geotechnical and Geoenvironmental Engineering 144 (10) (oct 2018). doi:10.1061/(asce)gt.1943-5606.0001958.

[34] W. Brząkała, Stress-weighted spatial averaging of random fields in geotechnical risk assessment, Studia Geotechnica et Mechanica 43 (4) (2021) 465–478. doi:10.2478/sgem-2021-0039.

[35] M. Lloret-Cabot, M. A. Hicks, A. P. van den Eijnden, Investigation of the reduction in uncertainty due to soil variability when conditioning a random field using kriging, Géotechnique Letters 2 (3) (2012) 123–127. doi:10.1680/geolett.12.00022.

[36] X. Y. Li, L. M. Zhang, J. H. Li, Using conditioned random field to characterize the variability of geologic profiles, Journal of Geotechnical and Geoenvironmental Engineering 142 (4) (apr 2016). doi:10.1061/(asce)gt.1943-5606.0001428.

[37] S.-H. Jiang, J. Huang, F. Huang, J. Yang, C. Yao, C.-B. Zhou, Modelling of spatial variability of soil undrained shear strength by conditional random fields for slope reliability analysis, Applied Mathematical Modelling 63 (2018) 374–389. doi:10.1016/j.apm.2018.06.030.

[38] J. Ding, J. Zhou, W. Cai, An efficient variable selection-based Kriging model method for the reliability analysis of slopes with spatially variable soils, Reliability Engineering & System Safety 235 (2023) 109234. doi:10.1016/j.ress.2023.109234.

[39] M. Chwała, Undrained bearing capacity of spatially random soil for rectangular footings, Soils and Foundations 59 (5) (2019) 1508–1521. doi:10.1016/j.sandf.2019.07.005.

[40] M. Chwała, M. Kawa, Random failure mechanism method for assessment of working platform bearing capacity with a linear trend in undrained shear strength, Journal of Rock Mechanics and Geotechnical Engineering 13 (6) (2021) 1513–1530. doi:10.1016/j.jrmge.2021.06.004.

[41] W.-K. Chen, Limit analysis and soil plasticity, Elsevier Scientific Pub. Co., 1975.

[42] S. Pietruszczak, Fundamentals of plasticity in geomechanics, Taylor & Francis Group, 2020.

[43] E. Vanmarcke, Random fields: Analysis and synthesis, World Scientific, 2010. doi:10.1142/5807.

[44] M. Chwała, Soil sounding location optimisation for spatially variable soil, Géotechnique Letters 10 (3) (2020) 409–418. doi:10.1680/jgele.20.00012.

[45] M. Chwała, Optimal placement of two soil soundings for rectangular footings, Journal of Rock Mechanics and Geotechnical Engineering 13 (3) (2021) 603–611.

[46] M. Chwała, D. J. Jerez, H. A. Jensen, M. Beer, Performance assessment of borehole arrangements for the design of rectangular shallow foundation systems, Journal of Rock Mechanics and Geotechnical Engineering (jul 2023). doi:10.1016/j.jrmge.2023.05.009.

[47] D. J. Jerez, H. A. Jensen, M. Beer, J. Chen, Asymptotic Bayesian Optimization: A Markov sampling-based framework for design optimization, Probabilistic Engineering Mechanics 67 (2022) 103178. doi:10.1016/j.probengmech.2021.103178.

[48] H. A. Jensen, D. J. Jerez, M. Valdebenito, An adaptive scheme for reliability-based global design optimization: A Markov chain Monte Carlo approach, Mechanical Systems and Signal Processing 143 (2020) 106836. doi:10.1016/j.ymssp.2020.106836.

[49] J. Ching, K.-K. Phoon, A. W. Stuedlein, M. Jaksa, Identification of sample path smoothness in soil spatial variability, Structural Safety 81 (2019) 101870. doi:10.1016/j.strusafe.2019.101870.

[50] Y. Li, J. Li, N. Xu, G. A. Fenton, P. J. Vardon, M. A. Hicks, On worst-case correlation length in probabilistic 3D bearing capacity assessments, Georisk: Assessment and Management of Risk for Engineered Systems and Geohazards (2022) 1–11doi:10.1080/17499518.2022.2132262.

[51] W. Puła, M. Chwała, On spatial averaging along random slip lines in the reliability computations of shallow strip foundations, Computers and Geotechnics 68 (2015) 128–136. doi:10.1016/j.compgeo.2015.04.001.

[52] S. Gourvenec, M. Randolph, O. Kingsnorth, Undrained bearing capacity of square and rectangular footings, International Journal of Geomechanics 6 (3) (2006) 147–157. doi:10.1061/(asce)1532-3641(2006)6:3(147).

[53] M. Chwała, On determining the undrained bearing capacity coefficients of variation for foundations embedded on spatially variable soil, Studia Geotechnica et Mechanica 42 (2) (2020) 125–136. doi:10.2478/sgem-2019-0037.

[54] G. S. Fishman, Monte Carlo: Concepts, algorithms and apllications, Springer New York, 1996. doi:10.1007/978-1-4757-2553-7.

[55] J. C. Spall, Introduction to Stochastic Search and Optimization, John Wiley & Sons, Inc., 2003. doi:10.1002/0471722138.

[56] D. J. Jerez, H. A. Jensen, M. Beer, A two-phase sampling approach for reliability-based optimization in structural engineering, in: Y. Liu, D. Wang, J. Mi, H. Li (Eds.), Advances in Reliability and Maintainability Methods and Engineering Applications, Springer Series in Reliability Engineering, Springer Nature Switzerland, 2023, pp. 21–48. doi:10.1007/978-3-031-28859-3_2.

[57] S. Kirkpatrick, C. D. Gelatt, M. P. Vecchi, Optimization by simulated annealing, Science 220 (4598) (1983) 671–680. doi:10.1126/science.220.4598.671.

[58] K. M. Zuev, J. L. Beck, Global optimization using the asymptotically independent Markov sampling method, Computers & Structures 126 (2013) 107–119. doi:10.1016/j.compstruc.2013.04.005.

[59] J. Wang, L. S. Katafygiotis, Reliability-based optimal design of linear structures subjected to stochastic excitations, Structural Safety 47 (2014) 29 – 38. doi:10.1016/j.strusafe.2013.11.002.

[60] J. Ching, Y.-C. Chen, Transitional Markov chain Monte Carlo method for Bayesian model updating, model class selection, and model averaging, Journal of Engineering Mechanics 133 (7) (2007) 816–832. doi:10.1061/(ASCE)0733-9399(2007)133:7(816).

[61] N. Metropolis, A. W. Rosenbluth, M. N. Rosenbluth, A. H. Teller, E. Teller, Equation of state calculations by fast computing machines, The Journal of Chemical Physics 21 (6) (1953) 1087–1092. doi:10.1063/1.1699114.

[62] W. K. Hastings, Monte Carlo sampling methods using Markov chains and their applications, Biometrika 57 (1) (1970) 97–109. doi:10.2307/2334940.

[63] P. Angelikopoulos, C. Papadimitriou, P. Koumoutsakos, X-TMCMC: Adaptive kriging for Bayesian inverse modeling, Computer Methods in Applied Mechanics and Engineering 289 (2015) 409–428. doi:10.1016/j.cma.2015.01.015.

[64] T. J. Santner, B. J. Williams, W. I. Notz, The design and analysis of computer experiments, Springer-Verlag GmbH, 2018.

[65] H. B. Nielsen, S. N. Lophaven, J. Søndergaard, DACE - A Matlab kriging toolbox, Tech. rep., Technical University of Denmark (DTU) (2002).